MicroRNA Signatures Associated with Basal Cell Carcinoma Subtypes

Suzanne Fastner[1,5], Hafeez Rahman[1,5], Jose Gutierrez[2], Nathan Shen[1], Scott R. Florell[3], Abigail Florell[3], Chris J. Stubben[1], Kenneth M. Boucher[1,4], Dekker C. Deacon[1,3], Robert L. Judson-Torres[1,3] and Douglas Grossman[1,3]

Basal cell carcinoma (BCC) is classified histologically into subtypes that determine treatment decisions. MicroRNAs (miRs) are short noncoding RNAs that may serve as diagnostic biomarkers. We investigated if particular miRs could distinguish BCC subtypes. We sequenced miRs from 55 archival BCC and 9 control skin specimens and then validated these miRs by qRT-PCR assay on a second BCC cohort (18 superficial, 16 nodular, 15 infiltrative) and control skin (n = 12). Expression values for individual miRs were normalized to miR-16-5p, which was the least variant among the control skin and BCC samples. We found that (i) miR-383-5p and miR-145-5p are downregulated in all BCC subtypes compared with control skin, (ii) miR-181c-5p is downregulated in superficial compared with invasive (nodular/infiltrative) BCC, and (iii) miR-22-5p and miR-708-5p are upregulated in infiltrative compared with superficial/nodular BCC and miR-30c-5p is downregulated in infiltrative compared with nodular BCC. Receiver operating characteristic analysis demonstrated excellent capacity of these miRs to discriminate between BCC and control skin (area under the curve, 0.94−0.98), whereas the capacity to discriminate between superficial and invasive subtypes was less robust (area under the curve, 0.7−0.8). Future prospective studies may determine the utility of these miRs as diagnostic biomarkers to guide biopsy and treatment of BCC.

Keywords: BCC, miRNA, Sequencing, Signature, Subtype

JID Innovations (2024);**4:**100286 doi:10.1016/j.xjidi.2024.100286

INTRODUCTION

Basal cell carcinoma (BCC) is classified histologically into subtypes (Figure 1) that guide treatment decisions. Tumors confined to the epidermis (eg, superficial BCC) are usually treated nonsurgically by curettage or with topical therapy, whereas invasive tumors usually require surgery to achieve high cure rates (Dawe, 2009). Invasive BCC is categorized primarily by morphology (eg, nodular, micronodular, infiltrative), and these categorizations generally correlate with risk of recurrence (Pyne et al, 2018). The underlying molecular basis for these subtypes, however, has not been well characterized.

MicroRNAs (miRs) are short noncoding RNAs that exhibit tissue-, neoplastic-, and cell type−specific expression patterns (Budakoti et al, 2021), and their small size allows for efficient recovery from archived samples and identification by sequencing (Cummins and Velculescu, 2006). Several miRs may serve as diagnostic biomarkers to distinguish nevi and melanomas (Torres et al, 2020). Prior reports have suggested miRs could offer a similar utility in the diagnosis of BCC (Tamas et al, 2021), but the few studies profiling miRs in BCC subtypes are limited by small sample sizes and the lack of secondary validation studies.

We sought to determine miR signatures associated with BCC subtypes from archival biopsy specimens.

RESULTS

Tumors demonstrating a single subtype were selected, representing 55 BCC (13 superficial, 10 nodular, 10 micronodular, and 22 infiltrative). In addition, we identified specimens of normal skin from BCC (n = 9) excisions that were free of scar or residual tumors to serve as controls. RNA was isolated and then subjected to miR-directed Illumina sequencing and analysis. Principal component analysis based on miR expression demonstrated striking segregation of all BCC tumors from control skin and segregation of superficial and infiltrative BCC subtypes from overlapping nodular and micronodular subtypes (Figure 2a). A heat map showing the clustering of tumor subtypes is provided in Figure 2b.

We initially examined the 10 possible pairwise subtype comparisons (eg, superficial vs infiltrative) and found a subset of miRs that were significantly different between each subtype (or control) pair. Consistent with the results of the principal component analysis, the nodular and micronodular

[1]*Huntsman Cancer Institute, University of Utah Health Sciences Center, Salt Lake City, Utah, USA;* [2]*University of Utah School of Medicine, Salt Lake City, Utah, USA;* [3]*Department of Dermatology, University of Utah Health Sciences Center, Salt Lake City, Utah, USA; and* [4]*Department of Medicine, University of Utah Health Sciences Center, Salt Lake City, Utah, USA*

[5]*These authors contributed equally to this work.*

Correspondence: Doug Grossman, Huntsman Cancer Institute, 2000 Circle of Hope, Salt Lake City, Utah 84112, USA. E-mail: doug.grossman@hci.utah.edu

Abbreviations: AUC, area under the curve; BCC, basal cell carcinoma; Ct, cycle threshold; miR, micro-RNA; ROC, receiver operating characteristic

Received 27 October 2023; revised 20 March 2024; accepted 31 March 2024; accepted manuscript published online XXX; corrected published online XXX

Cite this article as: JID Innovations 2024;4:100286

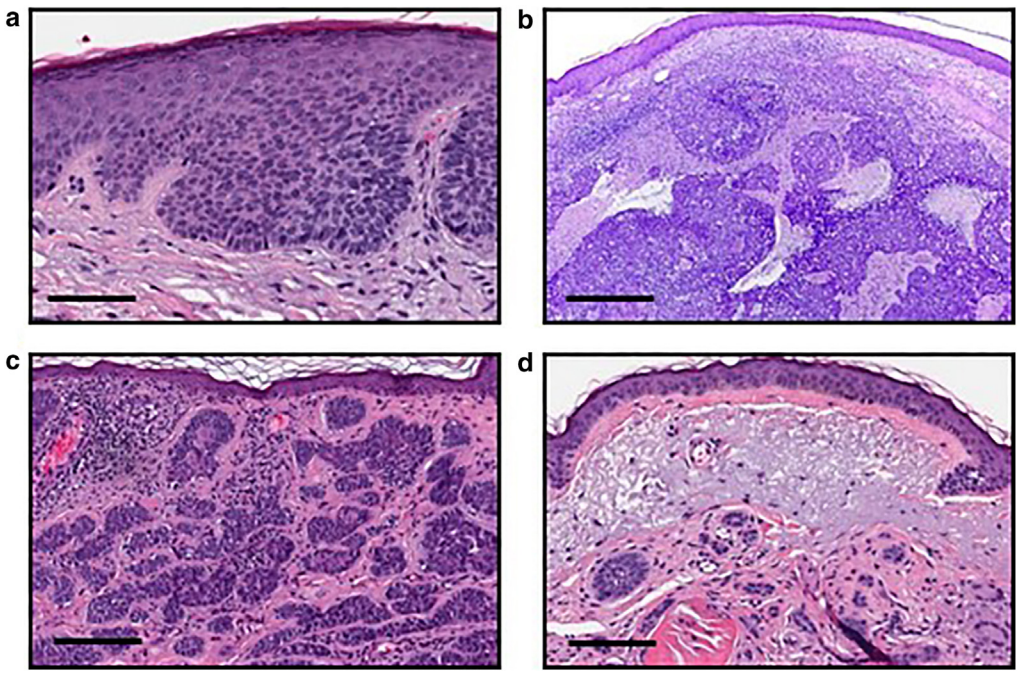

Figure 1. Histologic patterns of BCC. (**a**) In superficial BCC, tumor buds extend off the epidermis. (**b**) In nodular BCC, single nodule invades the dermis. (**c**) In micronodular BCC, small tumor aggregates in the dermis. (**d**) In infiltrative BCC, small strands of tumor cells in the deep dermis appear with scar-like stroma. BCC, basal cell carcinoma. Bars = 50 mm.

subtypes (101 miRs) were most similar, whereas the infiltrative and control samples (570 miRs) were most dissimilar (Table 1). Our classification strategy was three-pronged: (i) to identify miRs discriminating between BCC and control skin, (ii) to identify miRs discriminating between superficial and invasive (nodular/micronodular, infiltrative) BCC, and (iii) to identify miRs discriminating between infiltrative and other BCC subtypes (Figure 2c). We identified 11 miRs that showed the most significant differential expression between all BCC subtypes and control samples (miR-383-5p, miR-4705, and miR-145-5p), superficial subtype and other BCC subtypes (miR-181c-5p, miR-181b-5p, and miR-95-3p), infiltrative subtype and other BCC subtypes (miR-22-5p, miR-18a-3p, and miR-708-5p), and infiltrative and nodular or

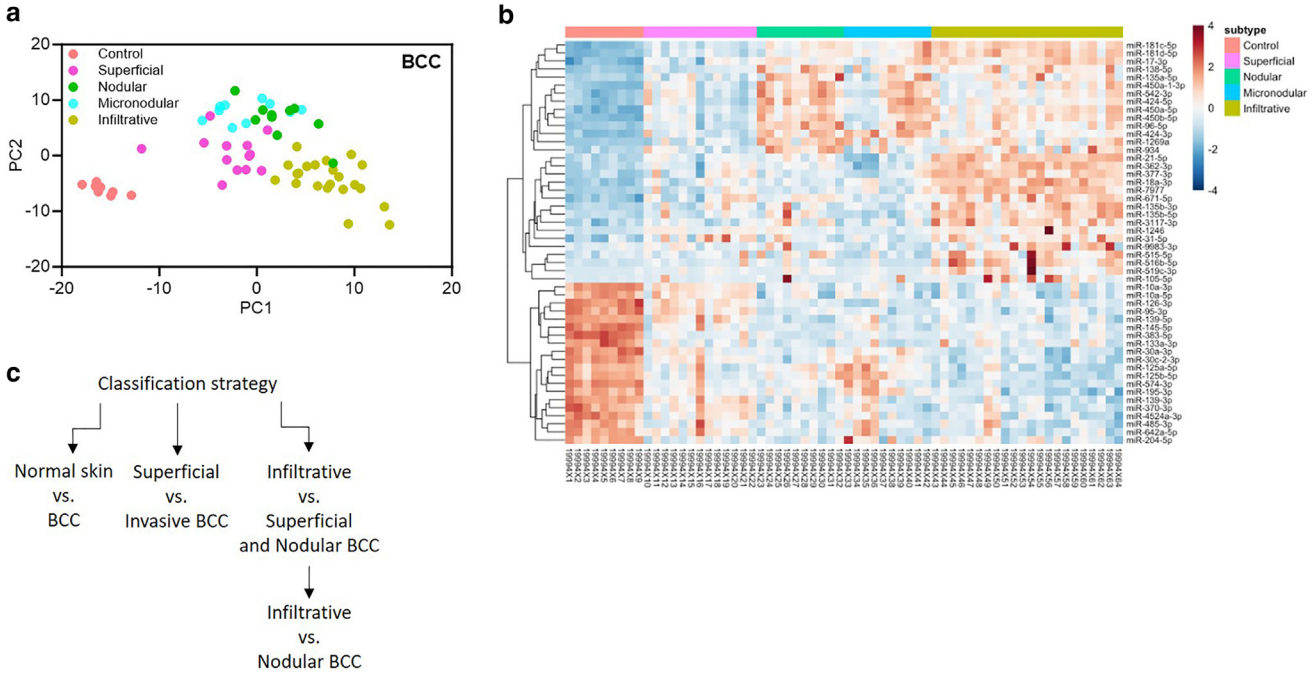

Figure 2. miR expression patterns in BCC subtypes and classification strategy. (**a**) Principal component analysis of miRs identified by sequencing of 55 BCC (n = 13 superficial, 10 nodular, 10 micronodular, and 22 infiltrative) and normal skin from BCC excisions (n = 9) that were free of scar or residual tumor. (**b**) Heat map showing hierarchical cluster analysis of the 50 miRs (y-axis) with the highest absolute values from the eigenvectors on PC1. The x-axis refers to the sample names, which are color-coded at the top. The color key represents Z-scores since the clustered regularized log values from DESeq2 are scaled by rows. (**c**) Classification strategy. BCC, basal cell carcinoma; PC, principal component.

Table 1. Pairwise Comparisons of miRNA Expression in BCC Subtypes and Control Samples

Pairwise Comparison[1]	miRs Up	miRs Down
Superficial vs control	189	151
Superficial vs nodular	93	90
Superficial vs micronodular	70	97
Superficial vs infiltrative	120	169
Nodular vs control	238	190
Nodular vs micronodular	49	52
Nodular vs infiltrative	152	191
Micronodular vs control	222	157
Micronodular vs infiltrative	178	210
Infiltrative vs control	340	230

BCC, basal cell carcinoma; miRs, microRNAs.
[1]For each pairwise comparison, there was a cutoff of adjusted $P < .05$.

micronodular subtypes (miR-758-3p and miR-30c-5p) as shown in Table 2. We also identified a miR (16-5p) that was the least variant in expression among the BCC and control skin samples to serve as an internal reference control.

To validate these BCC subtype miR signatures, we assembled a second distinct cohort of archival specimens representing 49 single BCC subtypes (18 superficial, 16 nodular, and 15 infiltrative) and control skin associated with BCC excisions (12) and used TaqMan Advanced probes (Thermo Fisher Scientific) corresponding to the 12 miRs for qRT-PCR analysis. Of the three miRs initially identified as downregulated in tumors versus control skin, in the validation cohort, expression of miR-383-5p and miR-145-5p was significantly lower in each BCC subtype compared with control skin (Figure 3a), whereas miR-4705 was not detected in any samples (not shown). Of the two miRs initially identified as downregulated in superficial versus other BCC, miR-181c-5p expression was significantly lower in superficial versus nodular and infiltrative BCC, and miR-181b-5p expression was significantly lower in superficial versus infiltrative (but not nodular) BCC (Figure 3b). Although miR-95-3p was initially identified as upregulated in superficial versus other BCC, it was not significantly different in superficial versus either nodular or infiltrative BCC (Figure 3b). For the four miRs initially identified as upregulated in infiltrative versus other BCC, expression of miR-22-5p and miR-758-3p was significantly higher in infiltrative BCC versus nodular and superficial BCC, and expression of miR-18a-3p and miR-708-5p was significantly higher in infiltrative versus superficial (but not nodular) BCC (Figure 3c). Finally, although miR-30c-5p was initially identified as downregulated in infiltrative versus nodular/micronodular BCC, its expression in the validation cohort was not significantly different among these subtypes (Figure 3c).

We considered that some results could be affected by potential differences in input miR quantity and quality as well as individual PCR reaction conditions. To address this possibility, we normalized the expression values for all the samples in the validation cohort using the least variant miR (miR-16-5p) and used these normalized expression values for the remainder of the analyses. Considering first the two miRs discriminating between control skin and all BCC subtypes, normalized expression of both miR-383-5c (Figure 4a) and miR-145-5p (Figure 4b) was significantly lower in all BCC subtypes compared with control skin. Similar results were obtained using a combined expression score for both miRs (Figure 4c). We next evaluated the receiver operating characteristic (ROC) of each miR using both individual normalized expression and combined expression scores and found that miR-383-5c was marginally better than miR-145-5p (area under the curve [AUC], 0.983 and 0.939, respectively) in discriminating between control skin and all BCC, and the combination of miR-383-5c and miR-145-5p was similar to miR-383-5c alone (AUC 0.986 and 0.983, respectively) (Figure 4d).

Next, considering the three miRs discriminating between superficial and nodular/infiltrative BCC subtypes, the normalized expression of miR-181c-5p (Figure 5a) was significantly lower in superficial BCC compared with nodular and infiltrative BCC, whereas the normalized expression of miR-181b-5p (Figure 5b) and miR-95-3p (Figure 5c) subtypes was not significantly different. For combined expression scores of miR-181c-5p and miR-181b-5p (Figure 5d), miR-181c-5p and miR-95-3p (Figure 5e), and all three miRs (Figure 5f), only the combined score of all three miRs was significantly different between superficial and nodular/infiltrative subtypes. Finally, ROC analyses revealed that the normalized expression of miR-181c-5p was superior to any of the combined expression scores (AUC 0.751, 0.717, 0.697, and 0.719, respectively) (Figure 5g).

Considering finally the five miRs potentially discriminating between infiltrative BCC and other subtypes, normalized expression of miR-22-5p (Figure 6a) and miR-708-5p (Figure 6b) was significantly greater in infiltrative BCC compared with superficial/nodular subtypes, and miR-30c-5p was significantly lower in infiltrative BCC compared with nodular BCC (Figure 6c). On the other hand, normalized expression of miR-758-3p (Figure 6d) and miR-18a-3p (Figure 6e) was not significantly different in infiltrative compared with nodular and superficial/nodular subtypes, respectively. For the various combined expression scores of these miRs, only that of miR-22-5p and miR-708-5p was statistically different in infiltrative compared with superficial/nodular subtypes (Figure 6f). Finally, among the statistically significant individual and combined expression scores, ROC analyses revealed that miR-22-5p was superior to the others (AUC 0.777 vs 0.626, 0.735) in discriminating infiltrative from superficial/nodular subtypes and that miR-30c-5p demonstrated superior performance (AUC 0.808) in discriminating infiltrative from nodular subtypes (Figure 6g).

DISCUSSION

In summary, we identified differential expression of several miRs in BCC and control skin and among BCC subtypes from sequencing of archival specimens, and most were validated in a second separate cohort by qRT-PCR assay. First, miR-383-5p and miR-145-5p are downregulated in all BCC subtypes compared with control skin, and both can individually discriminate between these entities with ROC AUCs > 0.94. Second, miR-181c-5p is downregulated in superficial compared with invasive (nodular/infiltrative) BCC and was able to discriminate between these two subtype categories

Table 2. Top Ranking miRs with Differential Expression in BCC Subtypes[1] and Control[2] Samples

miR	Comparison	Control	Sup	Nod	Micronod	Infil	*P*-Value	Adjusted *P*-Value
383-5p	BCC vs control	**5.679**[3]	1.888	1.512	1.601	1.685	4.89 E-28	4.25 E-26
4705	BCC vs control	**3.039**	1.357	1.669	1.938	1.472	3.20 E-12	4.02 E-11
145-5p	BCC vs control	**14.083**	12.139	11.535	11.790	11.751	6.27 E-28	5.06 E-26
181c-5p	Superficial vs other BCC	5.860	**6.850**	7.751	7.853	8.280	1.98 E-19	1.87 E -16
181b-5p	Superficial vs other BCC	8.586	**9.133**	9.795	9.974	10.101	1.04 E-13	2.34 E-11
95-3p	Superficial vs other BCC	10.100	**9.172**	8.421	8.302	8.332	8.51 E-14	2.34 E-11
22-5p	Infiltrative vs other BCC	6.569	6.826	6.783	6.895	**8.196**	1.58 E-53	1.74 E-50
18a-3p	Infiltrative vs other BCC	3.104	4.088	3.882	4.168	**5.269**	8.30 E-25	1.52 E-22
708-5p	Infiltrative vs other BCC	10.124	10.494	10.163	10.285	**11.446**	5.46 E-18	5.46 E-16
758-3p	Infiltrative vs nodular	3.142	2.999	2.531	3.068	**3.612**	1.22 E-12	9.63 E-11
30c-5p	Infiltrative vs nodular/micronodular	13.332	12.976	13.293	13.573	**12.756**	7.79 E-19	1.35 E-16
16-5p	Least variant	17.261	17.132	17.363	17.032	16.803	0.15	0.25

BCC, basal cell carcinoma; Infil, infiltrative; Micronod, micronodular; Nod, nodular; Sup, superficial.
[1]Superficial, nodular, micronodular, and infiltrative BCC subtypes.
[2]Skin from BCC excisions without histologic evidence of residual tumor or scar.
[3]Relative mean log2 values. Boldface values highlight differences between groups for each miR.

individually (AUC 0.751) better than in combination (AUC 0.697–0.719) with others that were downregulated (miR-181b-5p) or upregulated (miR-95-3p) in superficial versus invasive BCC. Third, miR-22-5p and miR-708-5p are upregulated in infiltrative compared with superficial/nodular BCC and miR-30c-5p is downregulated in infiltrative compared

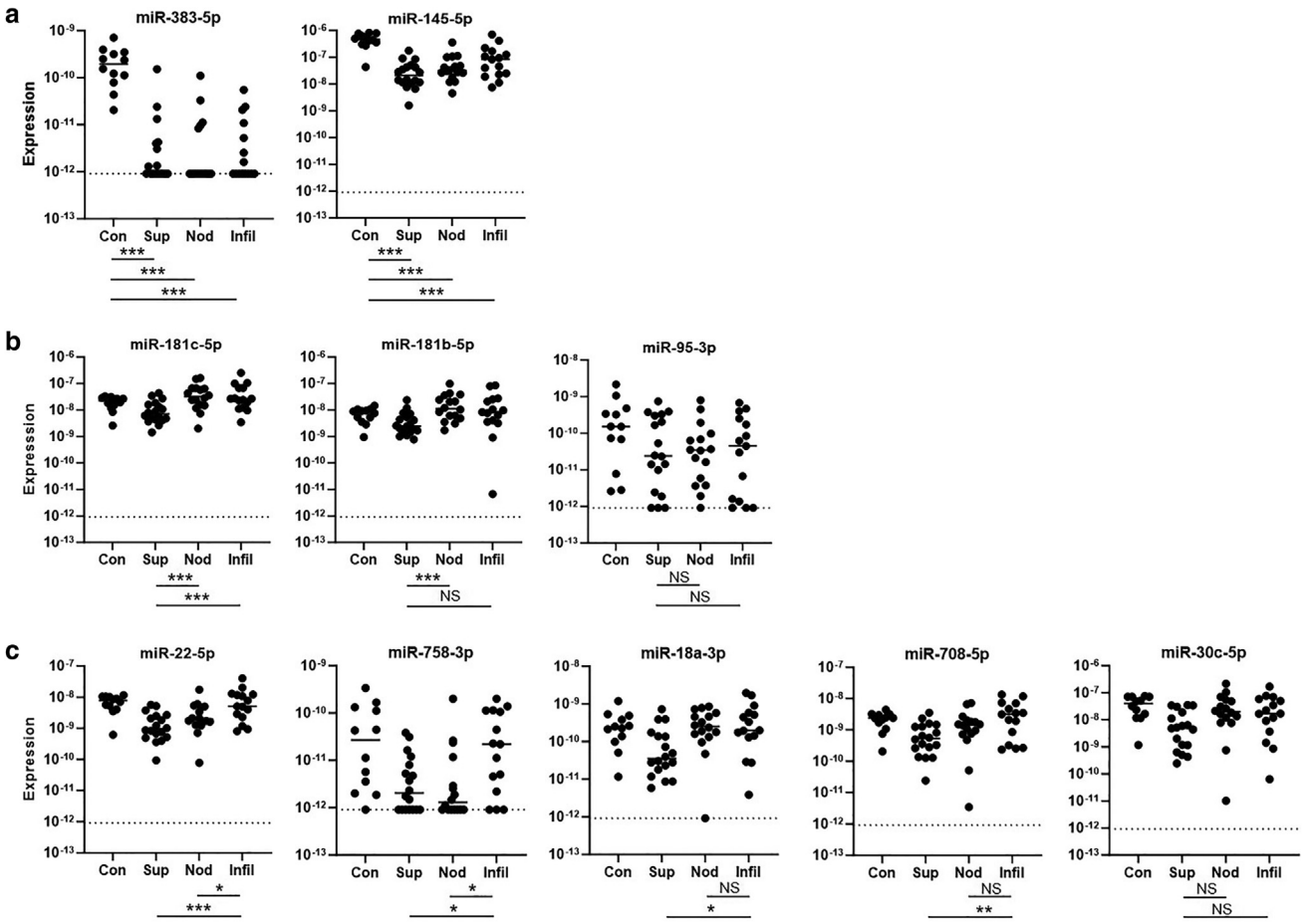

Figure 3. Expression of miRs in the validation cohort. Shown are non-normalized expression data for the indicated miRs selected to distinguish between (**a**) normal skin and BCC, (**b**) superficial from invasive BCC, and (**c**) infiltrative from nodular BCC in 12 control skin, 18 superficial, 16 nodular, and 15 infiltrative BCC samples. Raw Ct numbers were converted to expression values using the formula (2-Ct). Bars indicate median values. The dotted line in each plot represents the limit of detection (Ct = 40). ***$P < .001$, **$P < .01$, *$P < .05$; unpaired two-sided *t*-tests. BCC, basal cell carcinoma; Con, control; Ct, cycle threshold; Infil, infiltrative; miR, micro-RNA; Nod, nodular; NS, not significant; Sup, superficial.

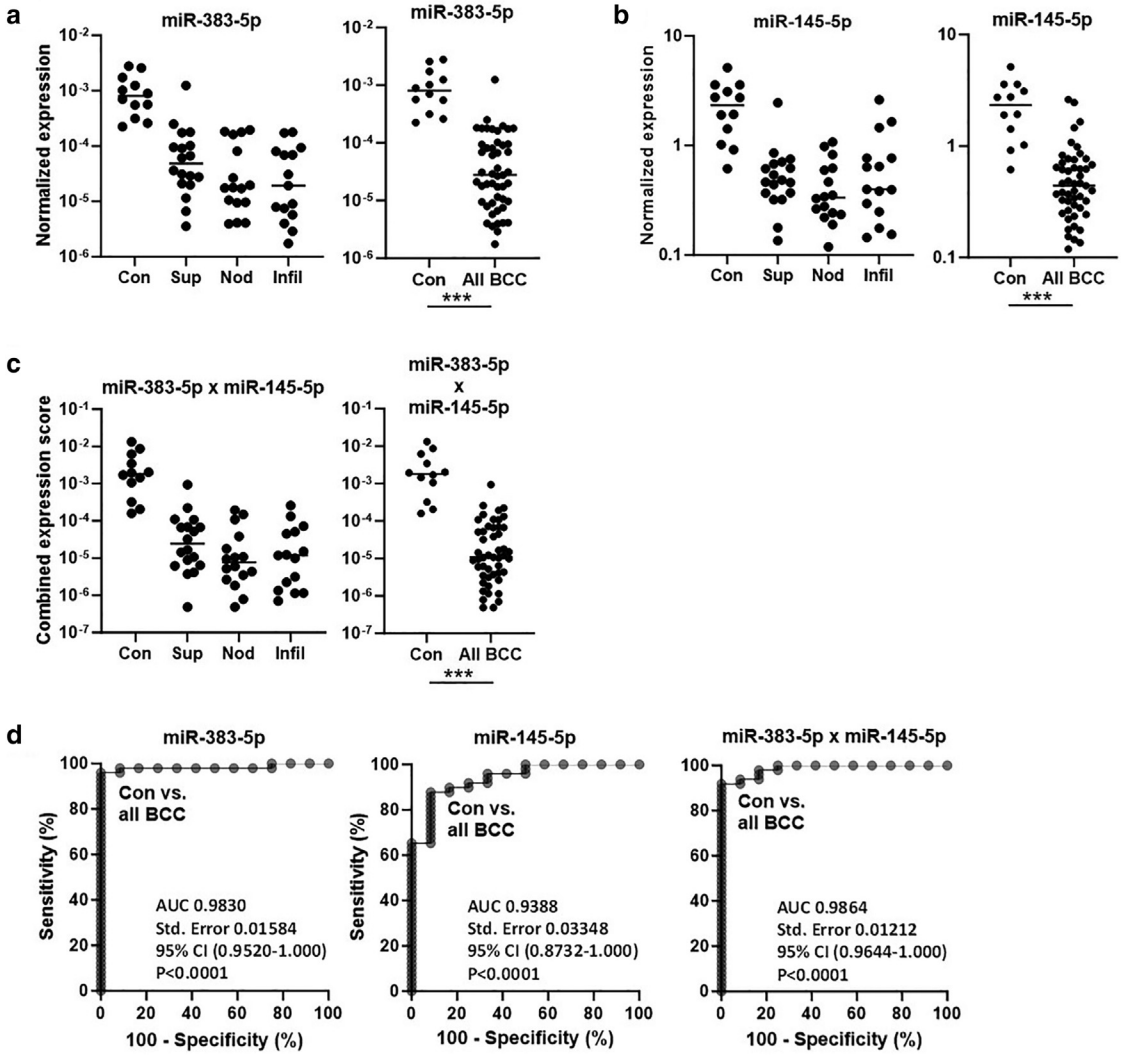

Figure 4. Validation of miRs distinguishing BCC from normal skin. Normalized expression values were obtained using the formula $2^{-(\text{Ct miR-16-5p subtracted from each Ct})}$ for 12 control skin, 18 superficial, 16 nodular, and 15 infiltrative BCC samples. Normalized expression of (**a**) miR-383-5p and (**b**) miR-145-5p in the separate cohorts (left panels) and control skin compared with all BCC (right panels). Bars indicate median values. ***$P < .001$, unpaired two-sided *t*-tests. (**c**) A combined expression score was obtained from the product of the normalized expression values for miR-383-5p and miR-145-5p and plotted for the separate cohorts (left panel) and in control skin compared with all BCC (right panel). Bars indicate median values. ***$P < .001$, unpaired two-sided *t*-test. (**d**) ROC curves for discrimination of control skin versus all BCC using normalized expression values as indicated for miR-383-5p and miR-145-5p individually, and combined expression scores for miR-383-5p and miR-145-5p. Values for AUC and 95% CI are shown, along with standard error and *P* values. AUC, area under the curve; BCC, basal cell carcinoma, CI, confidence interval; Ct, cycle threshold; Infil, infiltrative; miR, microRNA; Nod, nodular; ROC, receiver operating characteristic; Sup, superficial.

with nodular BCC, with miR-22-5p and miR-30c-5p able to discriminate between these subtype categories individually (AUC 0.777, 0.808) better than in combination (AUC 0.626, 0.735) with miR-708-5p. Several miRs (miR-181b-5p, miR-95-3p, miR-758-3p, and miR-18a-3p) identified as differentially expressed by sequencing were not validated by qRT-PCR in the second cohort, perhaps reflecting a true discrepancy or a technical issue related to the use of distinct detection platforms (Git et al, 2010).

To our knowledge, this study has investigated and validated miR expression differences on the largest number of control skin specimens and BCC tumors representing the different subtypes. Although most of the miRs presented here have not been previously reported in other work investigating miRs in BCC (Heffelfinger et al, 2012; Kashyap et al, 2022; Liu and Li, 2022; Renwick et al, 2013; Sonkoly et al, 2012; Tamas et al, 2021), most prior studies were limited by a small number of samples and/or did not differentiate by BCC subtype or include multiple subtypes. We did detect many of the previously reported miRs by sequencing but chose to pursue other miRs that demonstrated a greater magnitude of differential expression or statistical significance. One study identified miR-145-5p as downregulated and miR-181c-5p as upregulated in BCC compared with adjacent normal skin (Sand et al, 2012), consistent with our present findings.

Given the clinical use of a noninvasive test based on the expression of two RNAs captured on adhesive tape for

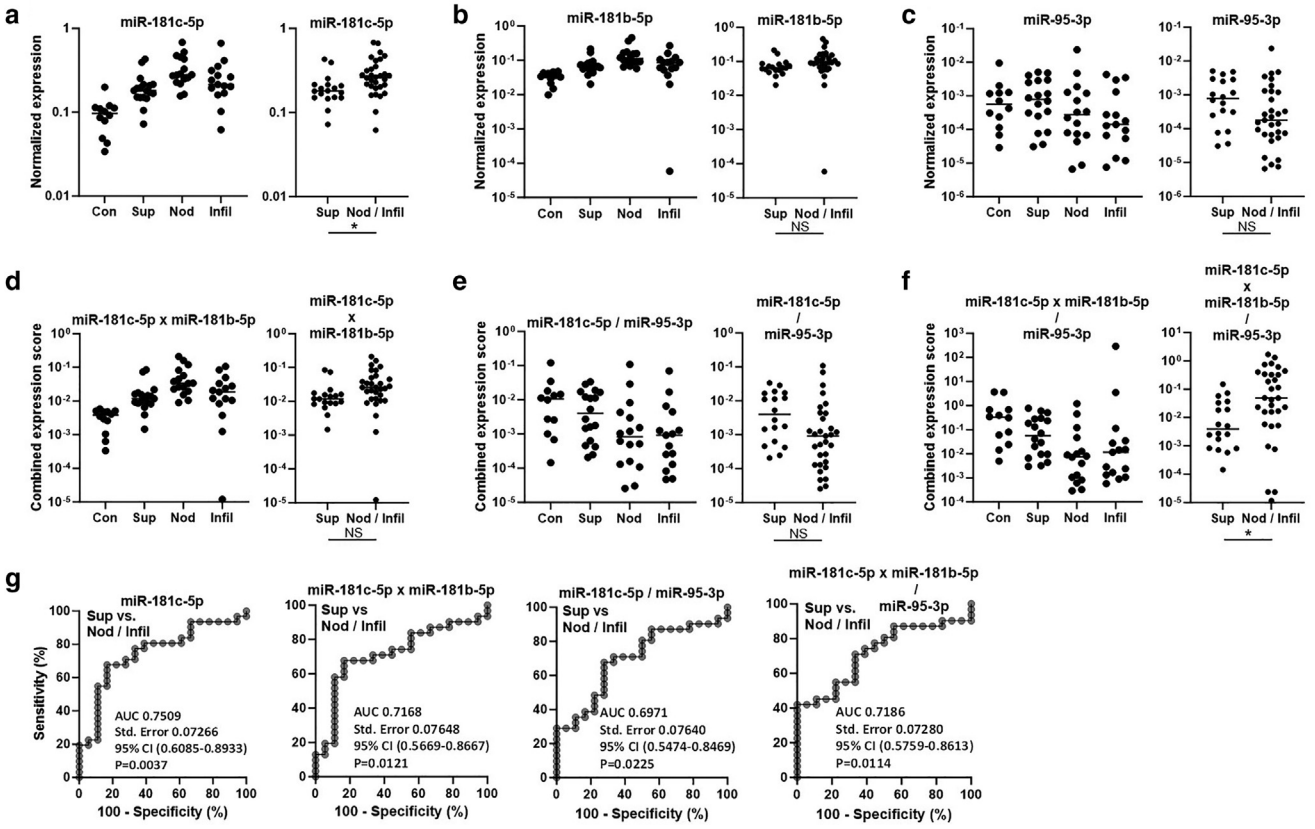

Figure 5. Validation of miRs distinguishing superficial from invasive BCC. Normalized expression values were obtained using the formula $2^{-(\text{Ct miR-16-5p subtracted from each Ct})}$ for 12 control skin, 18 superficial, 16 nodular, and 15 infiltrative BCC samples. Normalized expression of (**a**) miR-181c-5p, (**b**) miR-181b-5p, and (**c**) miR-95-3p in the separate cohorts (left panels) and control skin compared with all BCC (right panels). Bars indicate median values. *$P < .05$, unpaired two-sided *t*-tests. A combined expression score was obtained from (**d**) the product of normalized expression values for miR-181c-5p and miR-181b-5p, (**e**) normalized expression values for miR-181c-5p divided by those for miR-95-3p, and (**f**) product of the normalized expression values for miR-181c-5p and miR-181b-5p divided by those for miR-95-3p, and these combined scores were plotted for the separate cohorts (left panels) and in control skin compared with all BCC (right panels). Bars indicate median values. *$P < .05$, unpaired two-sided *t*-test. (**g**) ROC curves for discrimination of superficial vs. invasive (nodular and infiltrative) BCC using normalized expression score values as indicated for miR-181c-5p individually, and combined expression score values as indicated based on scores for miR-181c-5p, miR-181b-5p, and miR-95-3p. Values for AUC and 95% CIs are shown, along with standard error and *P* values. AUC, area under the curve; BCC, basal cell carcinoma, CI, confidence interval; Ct, cycle threshold; Infil, infiltrative; miR, micro-RNA; Nod, nodular; NS, not significant; ROC, receiver operating characteristic; Sup, superficial.

guiding biopsy decisions for pigmented lesions (Brouha et al, 2020), it is conceivable that a similar method based on miRs could be used to diagnose BCC and predict subtype before biopsy. For example, although miR-383-5p and miR-145-5p could be used to identify BCC and determine whether a biopsy is indicated, miR-181c-5p could be used to distinguish between superficial and invasive BCC that should be, respectively, biopsied using shave or punch technique, and a set of other miRs (miR-22-5p, miR-708-5p, and miR-30c-5p) could be used to identify infiltrative tumors that likely would require surgery to eradicate.

There are several limitations to our study that may restrict the general predictive utility of miRs before biopsy as discussed above. First, although we observed significant differences in the median expression values for several of these miRs in several subtypes, there was an overlap in their expression (particularly for miR-181c-5p) between the BCC subtypes. Further studies on a larger group of tumors would be required to determine the extent of variation for particular miRs. Second, we chose to normalize miRNA expression to the level of miR-16-5p, which is a well-known tumor suppressor miR that has been reported to be downregulated in nearly all examined malignant tissues (Ghafouri-Fard et al, 2022), including BCC (Sonkoly et al, 2012). However, in all of our included samples, tumors represented >80% of the tissue, and we determined that miR-16-5p was the least variable miR among the samples and therefore would be most appropriate for normalization. Indeed, we found more variability among samples in the initial analyses we performed without normalization. Finally, although our investigation was restricted to tumors, with each displaying a single subtype, in clinical practice, >20% of BCCs demonstrate more than one predominant subtype histologically or discordance between biopsy and subsequent excision specimens (Genders et al, 2016). Thus, future clinical development of this approach will depend on optimizing the discrimination of predominant subtypes in mixed tumors and may be limited to the differentiation of BCC from sun-damaged skin and nonmalignant skin tumors.

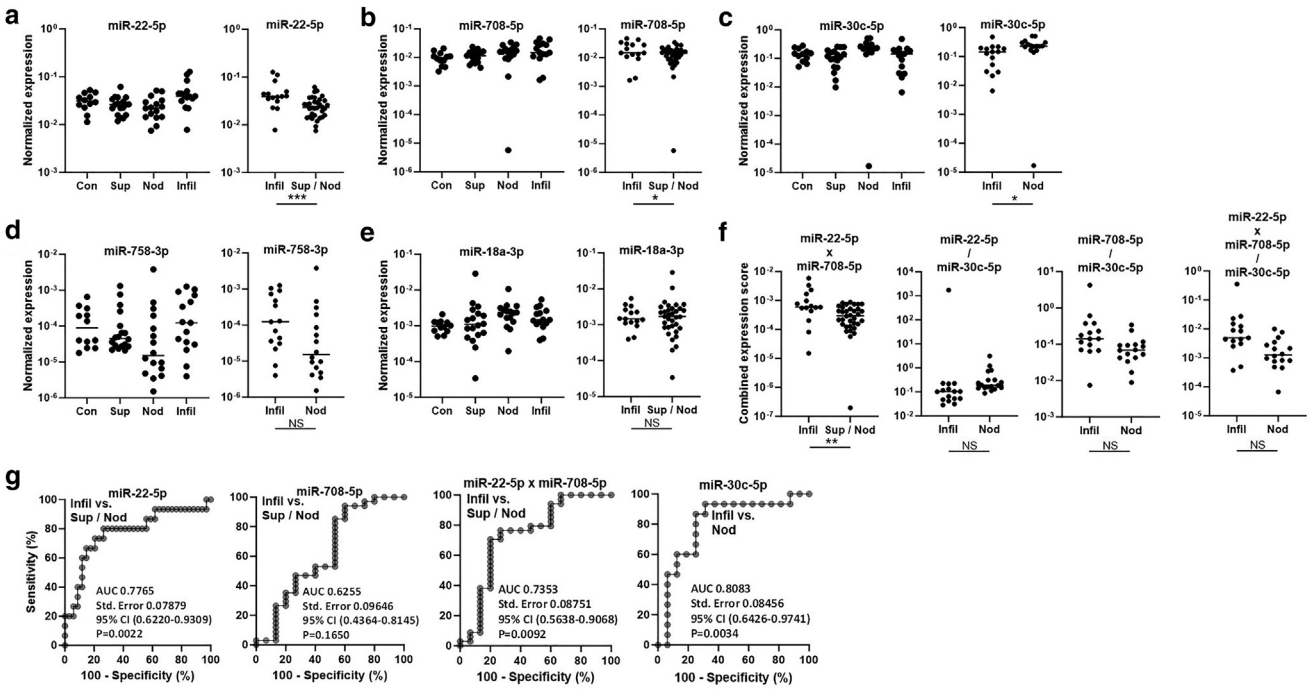

Figure 6. Validation of miRs distinguishing infiltrative from other BCC. Normalized expression values were obtained using the formula $2^{-(\text{Ct miR-16-5p subtracted from each Ct})}$ for 12 control skin, 18 superficial, 16 nodular, and 15 infiltrative BCC samples. Normalized expression of (**a**) miR-22-5p, (**b**) miR-708-5p, (**c**) miR-30c-5p, (**d**) miR-758-3p, and (**e**) miR-18a-3p in the separate cohorts (left panels) and in infiltrative BCC compared with superficial and nodular or nodular BCC as indicated (right panels). Bars indicate median values. ***$P < .001$, *$P < .05$; unpaired two-sided *t* tests. (**f**) Combined expression scores were obtained from the products and/or quotients of the normalized expression values for miR-22-5p, miR-708-5p, and miR-30c-5p, and plotted as indicated for infiltrative and superficial and nodular BCC or nodular BCC. Bars indicate median values. **$P < .01$, unpaired two-sided *t* test. (**g**) ROC curves for discrimination of infiltrative versus superficial and nodular BCC or versus nodular BCC, using individual normalized expression scores or combined expression scores for the indicated miRs. Values for AUC and 95% CIs are indicated, along with standard error and *P* values. AUC, area under the curve; BCC, basal cell carcinoma, CI, confidence interval; Ct, cycle threshold; Infil, infiltrative; miR, micro-RNA; Nod, nodular; NS, not significant; ROC, receiver operating characteristic; Sup, superficial.

MATERIALS AND METHODS

Cohort identification and RNA preparation for sequencing

Tumors were identified in the University of Utah Dermatopathology (PowerPath) database and corresponding H&E-stained slides were reviewed by a dermatopathologist (S.R.F.) to confirm the diagnosis, and tumors were selected that constituted >80% of the tissue specimen. Control specimens from BCC excisions were reviewed with a dermatopathologist (S.R.F.) and verified to be devoid of residual tumor or scar. Sections (20 mm) were cut, dried on glass slides, and then scraped into microfuge tubes. Whole RNA was isolated using a RecoverAll kit (Thermo Fisher Scientific, AM1975), quantitated by ScreenTape Assay (Agilent), and converted to cDNA (Qiagen QIAseq miRNA Library Prep) for sequencing.

miR sequencing

Sequencing was performed on an Illumina NovaSeq 6000 instrument in the High-Throughput Genomics Shared Resource at the Huntsman Cancer Institute. RNA concentration was measured with a Qubit RNA HS Assay Kit (Fisher Scientific #Q32855), and RNA quality was evaluated with an Agilent Technologies RNA ScreenTape Assay (5067-5579 and 5067-5580). Small RNA sequencing libraries were prepared from 10 to 100 ng of total RNA using the Qiagen QIAseq miRNA Library Kit (cat# 331505). Following PCR amplification, the library was size selected to enrich for adapter-ligated molecules encoding small RNA species using QIAseq magnetic beads. Size-selected libraries were qualified on an Agilent Technologies 4150 TapeStation High Sensitivity D1000 ScreenTape assay (5067-5584 and 5067-5585). The molarity of adapter-modified molecules was defined by quantitative PCR using the Kapa Biosystems Kapa Library Quant Kit (cat# KK4824). Individual libraries were normalized to 5 nM in preparation for Illumina sequence analysis.

Analysis of miR sequencing

The human Genome Reference Consortium human build 38 genome and gene annotation files were downloaded from Ensembl release 106, and a reference database was created using STAR version 2.7.9a (Dobin et al, 2013). A custom Perl script (smallRNA_pe_umi_extractor.pl from https://github.com/HuntsmanCancerInstitute/UMIScripts) was used to trim adapters and extract the Unique Molecular Index from the second read of a paired-end Qiagen small RNA library with 76 × 51 base pair reads. The trimmed reads were aligned to the reference database using STAR options optimized for shorter miRNA reads (≥16 bases matched to the genome, ≤5% mismatches over mapped length, splicing switched off). A second Perl script (bam_umi_dedup.pl) removed PCR duplicates from the aligned BAM file, and the mapped reads were assigned to annotated genes in Ensembl and to miRNAs in miRbase release 22.1 (Kozomara et al, 2019) using featureCounts version 1.6.3 (Liao et al, 2014). Differentially expressed miRNA in miRbase was identified using a 5% false

discovery rate with DESeq2 version 1.36.0 (Love et al, 2014). Principal component analysis was run using the regularized log values from the top 500 variable miRNAs.

Feature selection for miRs

Features (ie, miRs) were first normalized to have a standard deviation equal to one. Binomial lasso regression, as implemented in the R (version 4.0.2) package "glmnet" (Friedman et al, 2010), was then used to select a group of features that separated subtypes. Ten-fold cross-validation was used to select the penalty parameter for the lasso regression. The chosen penalty was one standard error from the parameter with the minimum cross-validated error. Features with nonzero model coefficients were ranked by the absolute value of the model coefficient. The Benjamini-Hochberg method was used for correcting *P*-values for multiple testing, as implemented by the "p.adjust" function in R.

qRT-PCR assays and analysis

Whole RNA was isolated as above, converted to cDNA using a TaqMan Advanced miRNA cDNA Synthesis Kit (Thermo Fisher Scientific, A28007), and TaqMan Advanced miRNA Assays were performed for each sample in triplicate, following manufacturer's directions (Thermo Fisher Scientific User Guide, A25576, Revision 3) with minor modifications. cDNA samples were diluted 1:100 in 0.1X Tris-EDTA buffer (2.5 μL final volume) and combined with 5 μL master mix (TaqMan Fast Advanced Master Mix, 4444557, Thermo Fisher Scientific), 2 μL RNAse-free water, and 0.5 μL selected hsa-miRNA probe (all from Thermo Fisher Scientific) and plated (final volume 10 μL) in a 384-well plate. Samples were run and analyzed on a C1000 Touch Thermo Cycler (Biorad, CFX384 Real-Time System). Cycle threshold (Ct) values from triplicates were averaged for further analysis using GraphPad Prism (version 10). Raw Ct numbers were converted to expression values using the formula (2^{-Ct}). Normalized expression values were obtained using the formula $2^{-(\Delta Ct)}$ where ΔCt represents the difference in Ct values for an individual miR and the invariant miR-16-5p. Combined expression scores were obtained from the products and/or quotients (based on whether miRs were "up" or "down," respectively) of normalized expression scores of two or three miRs. ROC curves and analyses were also generated using Prism software, based on previously described methods (Hanley and McNeil, 1982).

ETHICS STATEMENT

The protocol, in which patient consent was waived, was approved by the University of Utah Institutional Review Board (# 76927, subproject #91).

DATA AVAILABILITY STATEMENT

The miRNA sequencing dataset (accession # GSE245676) has been uploaded to GEO (https://www.ncbi.nlm.nih.gov/geo).

ORCIDs

Suzanne Fastner: http://orcid.org/0009-0002-5371-5985
Hafeez Rahman: http://orcid.org/0000-0001-6417-6011
Jose Gutierrez: http://orcid.org/0000-0002-7212-0816
Nathan Shen: http://orcid.org/0009-0006-8774-701X
Scott R. Florell: http://orcid.org/0000-0002-9502-1386
Abigail Florell: http://orcid.org/0009-0002-4402-3151
Chris J. Stubben: http://orcid.org/0000-0002-3390-4888
Kenneth M. Boucher: http://orcid.org/0000-0003-2833-0127
Dekker C. Deacon: http://orcid.org/0000-0002-4160-5730
Robert L. Judson-Torres: http://orcid.org/0000-0002-6559-0553
Douglas Grossman: http://orcid.org/0000-0003-1790-7023

CONFLICT OF INTEREST

The authors state no conflict of interest.

ACKNOWLEDGMENTS

We acknowledge support from the Department of Dermatology (D.G., D.C.D., and R.L.J-T.) at the University of Utah, the Huntsman Cancer Foundation and the National Cancer Institute (R01AR080626 to R.L.J-T.). This work was directly supported by a Translational Research award from the V Foundation. We utilized the High-Throughput Genomics, Bioinformatics Analysis, Cancer Biostatistics Shared Resources at Huntsman Cancer Institute at the University of Utah supported by the National Cancer Institute of the National Institutes of Health under Award Number P30CA042014.

AUTHOR CONTRIBUTIONS

Conceptualization: DCD, DG, RLJ-T; Formal Analysis: CJS, KMB; Funding Acquisition: DG, RLJ-T; Investigation: SF, NS, HR, JG, SRF, AF; Methodology: DG, RLJ-T; Supervision: DG; Writing - Original Draft Preparation: DG; Writing - Review and Editing: SF, NS, HR, JG, DCD, AF, SRF, CJS, KMB, DG, RLJ-T

DECLARATION OF GENERATIVE ARTIFICIAL INTELLIGENCE (AI) OR LARGE LANGUAGE MODELS (LLM)

The authors did not use AI/LLM in any part of the research process and/or manuscript preparation.

REFERENCES

Brouha B, Ferris LK, Skelsey MK, Peck G, Moy R, Yao Z, et al. Real-world utility of a non-invasive gene expression test to rule out primary cutaneous melanoma: a large US registry study. J Drugs Dermatol 2020;19:257–62.

Budakoti M, Panwar AS, Molpa D, Singh RK, Büsselberg D, Mishra AP, et al. Micro-RNA: the darkhorse of cancer. Cell Signal 2021;83:109995.

Cummins JM, Velculescu VE. Implications of micro-RNA profiling for cancer diagnosis. Oncogene 2006;25:6220–7.

Dawe RS. Treatment options for non-melanoma skin cancer. G Ital Dermatol Venereol 2009;144:453–8.

Dobin A, Davis CA, Schlesinger F, Drenkow J, Zaleski C, Jha S, et al. STAR: ultrafast universal RNA-seq aligner. Bioinformatics 2013;29:15–21.

Friedman J, Hastie T, Tibshirani R. Regularization paths for generalized linear models via coordinate descent. J Stat Softw 2010;33:1–22.

Genders RE, Kuizinga MC, Teune TM, van der Kruijk M, van Rengen A. Does biopsy accurately assess basal cell carcinoma (BCC) subtype? J Am Acad Dermatol 2016;74:758–60.

Ghafouri-Fard S, Khoshbakht T, Hussen BM, Abdullah ST, Taheri M, Samadian M. A review on the role of mir-16-5p in the carcinogenesis. Cancer Cell Int 2022;22:342.

Git A, Dvinge H, Salmon-Divon M, Osborne M, Kutter C, Hadfield J, et al. Systematic comparison of microarray profiling, real-time PCR, and next-generation sequencing technologies for measuring differential microRNA expression. RNA 2010;16:991–1006.

Hanley JA, McNeil BJ. The meaning and use of the area under a receiver operating characteristic (ROC) curve. Radiology 1982;143:29–36.

Heffelfinger C, Ouyang Z, Engberg A, Leffell DJ, Hanlon AM, Gordon PB, et al. Correlation of global microRNA expression with basal cell carcinoma subtype. G3 (Bethesda) 2012;2:279–86.

Kashyap MP, Sinha R, Mukhtar MS, Athar M. Epigenetic regulation in the pathogenesis of non-melanoma skin cancer. Semin Cancer Biol 2022;83:36–56.

Kozomara A, Birgaoanu M, Griffiths-Jones S. miRBase: from microRNA sequences to function. Nucleic Acids Res 2019;47:D155–62.

Liao Y, Smyth GK, Shi W. featureCounts: an efficient general purpose program for assigning sequence reads to genomic features. Bioinformatics 2014;30:923–30.

Liu F, Li S. Non-coding RNAs in skin cancers: biological roles and molecular mechanisms. Front Pharmacol 2022;13:934396.

Love MI, Huber W, Anders S. Moderated estimation of fold change and dispersion for RNA-seq data with DESeq2. Genome Biol 2014;15:550.

Pyne JH, Barr E, Myint E, Clark SP, David M, Na R. Invasive squamous cell carcinoma: comparison of differentiation grade and tumour depth by anatomical site in 1666 tumours. Clin Exp Dermatol 2018;43:3–10.

Renwick N, Cekan P, Masry PA, McGeary SE, Miller JB, Hafner M, et al. Multicolor microRNA FISH effectively differentiates tumor types. J Clin Invest 2013;123:2694–702.

Sand M, Skrygan M, Sand D, Georgas D, Hahn SA, Gambichler T, et al. Expression of microRNAs in basal cell carcinoma. Br J Dermatol 2012;167:847–55.

Sonkoly E, Lovén J, Xu N, Meisgen F, Wei T, Brodin P, et al. MicroRNA-203 functions as a tumor suppressor in basal cell carcinoma. Oncogenesis 2012;1:e3.

Tamas T, Baciut M, Nutu A, Bran S, Armencea G, Stoia S, et al. Is miRNA regulation the key to controlling non-melanoma skin cancer evolution? Genes (Basel) 2021;12:1929.

Torres R, Lang UE, Hejna M, Shelton SJ, Joseph NM, Shain AH, et al. MicroRNA ratios distinguish melanomas from nevi. J Invest Dermatol 2020;140:164–73.e7.